World Electric Vehicle Journal

MDPI

Article

Evaluating the Optimal Electric Vehicle Location for a Hybrid Energy System Controlled with Novel Active Disturbance Rejection Controller

Zahid Farooq [1], Sheikh Safiullah [1], Asadur Rahman [1,*], S. M. Suhail Hussain [2] and Taha Selim Ustun [3,*]

[1] Electrical Engineering Department, National Institute of Technology Srinagar, Srinagar 190006, Jammu and Kashmir, India
[2] Electrical Engineering Department, King Fahad University of Petroleum and Minerals, Daharan 31261, Saudi Arabia
[3] Fukushima Renewable Energy Institute, National Institute of Advanced Science and Technology (AIST), Koriyama 963-0298, Japan
* Correspondence: asadur2003@yahoo.co.in (A.R.); selim.ustun@aist.go.jp (T.S.U.)

Abstract: Power system control is an important issue with regard to power system safety, flexibility, and reliability. Over the years, various new power system control strategies have been explored, but the main disadvantage of these control strategies is their complexity in structures with respect to industrially applied PID controller. The present paper introduces a novel control strategy based on modified disturbance rejection control, which is a modification of the PID controller that not only preserves the simplicity of control design but also offers an effective control based on state observer-based control law. The proposed control strategy addresses some basic limitations of a PID controller and implements modified control law to remove these limitations. In order to prove the effective control of the proposed control strategy, a standard IEEE-39 bus power system integrated with renewable energy generations is developed, and a comparative analysis of the proposed controller is performed with respect to its ancestor controllers. The comparison is validated based on the system dynamic responses like frequency and tie-line power deviations when the power system is subjected to different disturbances. Furthermore, the power system is integrated with electric vehices (EVs) in vehicle-to-grid (V2G) mode in order to ascertain the effect of EVs when used in V2G mode. A novel study is carried out in which the optimal location of EVs in the power system is determined based on the enhancement in stability of the power system by EVs. The analyses are carried out in MATLAB Simulink software. Simulation reports reflect the optimal control action of the proposed controller with respect to already established strategies projected in the literature. Moreover, the results illustrate that EVs when connected in Area 1 and Area 3 of the power system, the system deviations and steady-state errors are much less as compared to the other cases.

Keywords: active disturbance rejection controller; electric vehicle; arithmetic optimization algorithm (AOA); integral squarred error (ISE); renewable energy sources

check for updates

Citation: Farooq, Z.; Safiullah, S.; Rahman, A.; Hussain, S.M.S.; Ustun, T.S. Evaluating the Optimal Electric Vehicle Location for a Hybrid Energy System Controlled with Novel Active Disturbance Rejection Controller. *World Electr. Veh. J.* **2022**, *13*, 192. https://doi.org/10.3390/wevj13100192

Academic Editor: Joeri Van Mierlo

Received: 1 September 2022
Accepted: 4 October 2022
Published: 17 October 2022

Publisher's Note: MDPI stays neutral with regard to jurisdictional claims in published maps and institutional affiliations.

Copyright: © 2022 by the authors. Licensee MDPI, Basel, Switzerland. This article is an open access article distributed under the terms and conditions of the Creative Commons Attribution (CC BY) license (https://creativecommons.org/licenses/by/4.0/).

1. Introduction

A large number of power-producing units must link via existing transmission lines to meet the increasing power demand. Controlling such a vast, interconnected power system in the face of rising scale and complexity has clearly become one of the most difficult tasks confronting the present-day power system. As the load demand on power systems is unpredictable and random, the system dynamics of frequency and tie-line power flow may diverge from their expected levels [1]. Hence, load frequency control (LFC) is critical for keeping these system dynamics at their desired levels [2–4]. The system responses may deteriorate due to inappropriate design of the LFC system, eventually leading to system

instability. Therefore, the present article intends to design an LFC system for efficacious frequency control approach for hybrid energy systems (HESs) [5,6].

One of the growing trends in the present area of research is the integration of electric vehicles (EVs) with power systems. The integration of EVs with power systems has proven to be an additional choice for improving the stability of power systems. As such, the present work gives a detailed analysis on the integration of EVs with the developed power system.

1.1. Background

A PID controller is the dominant controller used in industries. However, PID suffers from some major limitations, such as its linear control law, which cannot account for the nonlinear nature of the present power systems. Similarly, the derivative control has additional noise inheritance, which deteriorates the control action. Another limitation is the integral saturation approach of the PID controller. Hence, these limitations need to be addressed in order to achieve an effective power system control operation.

1.2. Related Works and Limitations

Elgerd et al. [7] presented the first attempt of frequency mitigation in multi-area (MA)-based power systems. Saika et al. [8] used the concept given by [7] to study LFC problems in several MA power systems. The reports published by [9,10] discussed the MA thermal system for LFC operation considering appropriate system nonlinearities for practical applications. The nonlinearities considered were generation rate constraint (GRC) and governor dead band (GDB). In recent times, the major source of power comes from thermal and hydro units. The report published by [11] demonstrated the LFC problem with hydro as a generation unit with applicable GRC. However, the reports [12–14] studied the LFC problem with hydro-thermal as generation sources along with system nonlinearities. The time delay, in addition to the GRC and GDB as nonlinearities for MA power systems, is illustrated in [15]. The reports [7–15] mentioned above mainly discuss the LFC problem with non-renewables. However, various factors, viz. the rapid rise in population and industrialization, have put an additional burden on the existing power system. Fossil fuels are being exhausted at a rapid pace, thereby prompting scholars to incorporate renewable-based power units into the existing power system [16]. Renewable energy sources (RES) are eco-friendly, and their performance is increasing at a rapid pace. In LFC analysis, wind and solar energy are the most common RES [17]. A detailed analysis of RES in effective frequency stabilization is discussed in [18]. Farooq et al. [19] used a solar thermal system (STS) for LFC operation of an MA power system and the authors in [20] have used a wind turbine system (WTS) in addition to the STS in the MA power system.

Geothermal energy (GTE) is one of the rapidly emerging RES that is being utilised to generate electricity all over the world. It is a form of thermal energy that is stored by nature in the Earth's core and is extracted directly whenever required. GTE generation differs from conventional generation in terms of unit size and dissolved particulate matter. They operate similarly to coal or nuclear power plants, with the exception of the heat source. Hermission, in his thesis [21], presented the dynamic control of frequency for both simulations and real-time measurements in power systems incorporating geothermal plants. The practical Icelandic PSS/E model was utilized for performing dynamic simulations of the power system. Tasnin, in his article [22], discussed a two-area deregulated power system. The authors in [23] presented the economic and ecological results of using the pump heat connected together with photovoltaic panels.

The power system is incorporated with the geothermal plant in addition to the DSTS and conventional thermal plant. The authors in [24] proposed a machine learning-based approach for energy management in renewable microgrids. The outcome from this article stated that GTPP effectively improved the system responses. From the literature mentioned above, some articles are available on frequency control of HESs with geothermal plants in addition to the WTS and STS. Hence, the authors are able to incorporate GTP in frequency control of HESs.

The atmosphere is being harmed by carbon emissions that comes from conventional transportation vehicles and power plants viz. thermal energy. In this respect, EVs are proving to be a feasible alternative for minimizing carbon emissions [25]. The extensive adoption of EVs allows for grid frequency regulation and a reduction in the power output of typical power-generating units [26]. EVs, in addition to STS and conventional thermal energy for effective frequency control of HES, is presented in [27].

The literature stated above shows that EVs in the present power system represent an evolving area of research. Therefore, the authors are in view to explore the EVs in the current power system.

The system responses in terms of frequency and tie-line power fluctuations diverge from their normal values after a disruption occurs in the power system. For such cases, control remains an uphill challenge. The utilization of modern control approaches significantly helps in frequency mitigation of HESs. Various articles in the literature have reported modern-day controlling approaches for performance improvement of HESs: cascaded ID-PD [4,27], integral double derivative (IDD) [8], fractional order depended integral and derivative (I^{λ} D^{μ}) [9], three degree of freedom PID (1DOF-PID) [10], PID [11,20], PI [12], dual-mode regulator [13], fuzzy PID [15], fuzzy IDD [19], FOPI-FOPD [22], two degree of freedom PID [28] and PI-(1+DD) [29] are designed for improved LFC control of HESs. An efficient active disturbance rejection control (ADRC) strategy for improved LFC strategy is efficiently discussed in [30]. The comparison of responses for ADRC against a PID controller showed significant enhancement in system dynamics. A robust adaptive control (RAC) utilization in automatic voltage regulator (AVR) is demonstrated by the authors in [31]. The results are significantly enhanced with RAC in contrast to the PID and FOPID controller. A robust disturbance-rejection-based controller for system performance improvement of HES is discussed in [32]. Fractional disturbance rejection-based control for effective system dynamic control of HES is demonstrated by [33]. From the reports discussed above, disturbance rejection-based controllers showed improved results against the conventional and other advanced controllers. Therefore, the authors get motivation to apply a disturbance rejection-based controller in HES.

The controller gains must be adjusted at their optimum values for efficacious operation of HESs. The meta-heuristc optimization approaches have been very effective in doing so [34–37]. Various optimization approaches are present in the literature satin bowerbird optimizer (SBO) [4], bacterial foraging (BF) [8], firefly algorithm [9,15], bio-geography-based optimization (BBO) [10,20,38,39], genetic algorithm (GA) [11,14], particle swarm optimization (PSO) [12,13], magnetotactic bacteria optimization (MBO) [40–42], sine cosine algorithm (SCA) [22], and the gravitational search algorithm (GSA) [32] for adjusting of different controller gains. An efficacious novel arithmetic optimization algorithm (AOA) [43] is discussed in studies that exhibited better outcomes in respect to other optimization approaches. Therefore, the current analysis uses the AOA approach for adjusting the controller gains.

1.3. Motivation

This research is supported by the fact that the majority of work reported in the literature has introduced very complex control strategies for power systems, which leads to the addition of complexity of the power systems. In addition, the established control strategies have only dealt with the known power system disturbances applied to the system without considering the impact of unknown model errors and uncertainties that emerge in the system. Moreover, the impact of electric vehicles and their optimal location for integration with the power system has never been thoroughly addressed. This work addresses these shortcomings appropriately because further advances in such areas need a base for power system design. Moreover, the integration of renewable energy sources is motivated by the fact that they provide faster response to the change in system load demand as compared to the conventional thermal plant, thus improving the stability time.

1.4. Contributions

The main contributions of the present work include the following.

1. This study introduces a robust control scheme based on system disturbance estimation and rejection. The proposed scheme takes into consideration both known disturbances subjected to the system as well as system uncertainties and unknown modelling errors to mitigate their effect on the performance of the developed HES.
2. The effect of linking EVs to hybrid energy system (HES) performance when connected to different buses of the IEEE-39 bus system is evaluated. Moreover, the optimal location of EVs for improved HES operation is examined.

1.5. Objectives

From the above discussions, the objectives for establishing the present work are as follows:

1. Development of a standard three-area HES integrated with modern day renewable sources for concurrent frequency and tie-line power control.
2. Development and implementation of modified robust control scheme in the form of first-order ADRC (1D-ADRC) for the performance increment of the HES and verification of its superiority with respect to applied control strategies available in the literature for establishing concurrent frequency and tie-line power control of the HES.
3. To investigate the impact of present-day EVs on the HES by connecting the EVs on different buses of the HES and to find the optimal location of EVs for improved operation of the HES.

2. Methodology Applied for the Present Work

In order to attain the required objectives discussed in above section, the details of the system investigated, the optimization technique used, and the implementation of proposed control strategy is discussed in this section.

2.1. Power System under Investigation

For establishing the optimal control action of the proposed controller, the proposed scheme is tested on a standard IEEE-39 bus system. Figure 1 shows the single-line diagram (SLD) of the developed power system. The power system is made more realistic by integrating the IEEE bus with solar, wind, and geothermal energy sources. The values considered for system parameters are taken form [44]. The test system under consideration has 10 generators (G1–G10), 39 buses, 12 transformers, 19 loads, and 34 transmission lines. All system nonlinearities and the speed governor for power generators are also considered. The test system is generally divided in three areas (Area 1, Area 2, and Area 3). It is assumed that only one generator is considered for the LFC task in each area. The generators include G1 in Area 1, G8 in area 2, and G5 in area 3. Figure 2 showcases the overall three-area HES considered. Each area in HES is comprised of several generation sources that includes both renewable and non-renewable energy sources. All three areas effectively take part in dynamic frequency regulation of HES. MATLAB Simulink software is applied to perform the overall analysis of HES.

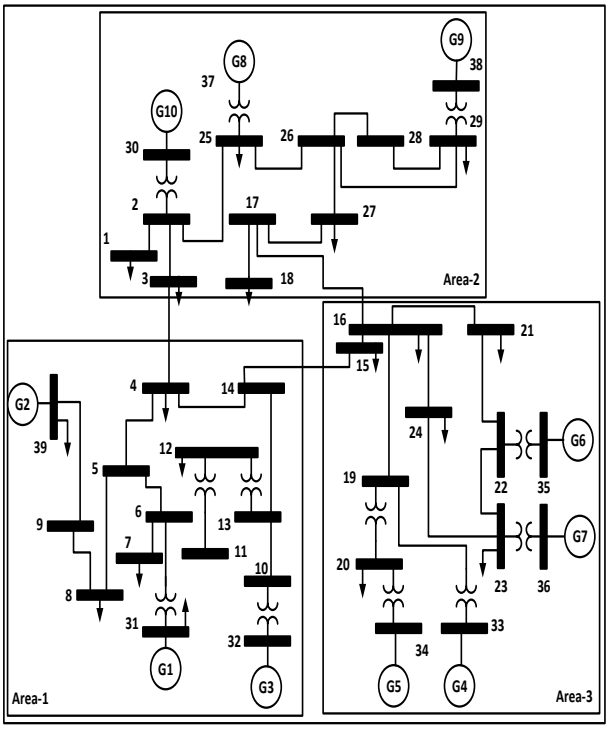


Figure 1. SLD of IEEE-39 bus system.

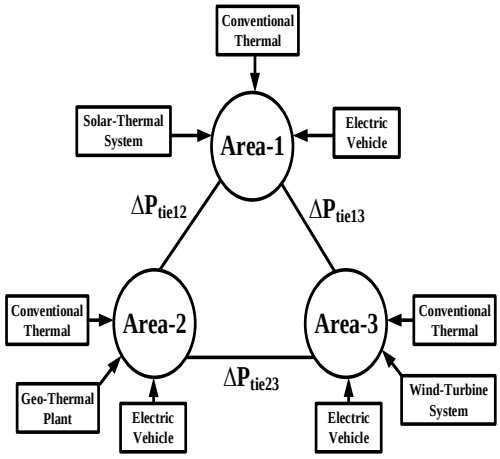


Figure 2. Interlinked three-area power system.

2.2. *Proposed First-Order Active Disturbance Rejection Controller (1D-ADRC) Modelling*

Consider a first-order system having gain = K, time constant = T as

$$P(s) = \frac{y(s)}{u(s)} = \frac{K}{Ts+1}. \tag{1}$$

Equation (1) can be written as

$$T\dot{y}(t) + y(t) = Ku(t). \tag{2}$$

When the system is subjected to a disturbance, $d(t)$, Equation (2) becomes

$$\dot{y}(t) = \frac{-1}{T}y(t) + \frac{1}{T}d(t) + \frac{K}{T}u(t) \tag{3}$$

$$= \frac{-1}{T}y(t) + \frac{1}{T}d(t) + bu(t), \tag{4}$$

where $b = K/T$.

The present HES has disturbance ($d(t)$) in the form of load variations (SLP), which is the known disturbance subjected to the system. However, apart from the known disturbance, some unknowns are also present in the system, which need to be taken into account. Hence, consider $b = b_0 + \Delta b$, where b_0 = known disturbance subjected to the HES and Δb is the unknown present in the HES. Thus, we obtain Equation (5):

$$\dot{y}(t) = \frac{-1}{T}y(t) + \frac{1}{T}d(t) + \Delta bu(t) + b_0u(t) \tag{5}$$

$$= f(t) + b_0u(t). \tag{6}$$

Equation (6) considers $f(t)$ to be a generalized disturbance by adding $(-1/T) \times y(t)$, $d(t)$ and Δb. Thus, Equation (6) models the process equivalent to a first-order low-pass filter.

The main feature of ADRC is to estimate the $f(t)$ by using a disturbance observer, called an extended state observer (ESO). The ESO helps in compensating the effect of $f(t)$ on the present HES. The remaining part can easily be handled by actual controller, like that of a proportional controller.

The ESO can be derived by using state-space analysis of the disturbed process from Equation (6):

$$\begin{aligned} \dot{x}(t) &= Ax(t) + Bu(t) + G\dot{f}(t) \\ y(t) &= Cx(t), \end{aligned} \tag{7}$$

where

$$\begin{aligned} &A = \begin{pmatrix} 0 & 1 \\ 0 & 0 \end{pmatrix}, B = \begin{pmatrix} b_0 \\ 0 \end{pmatrix}, G = \begin{pmatrix} 0 \\ 1 \end{pmatrix}, \\ &C = \begin{pmatrix} 1 & 0 \end{pmatrix} \end{aligned} \tag{8}$$

where $\dot{f}(t)$ is a sort of "virtual" input that cannot be measured as such. Hence, the ESO for such a process can be constructed by using $u(t)$ input and $y(t)$ output. The representation of ESO for such a process is given by Equation (9):

$$\begin{aligned} \dot{x}(t) &= Ax(t) + Bu(t) + L(y(t) - x_1(t)) \\ &= (A - L)x(t) + Bu(t) + Ly(t), \quad L = \begin{pmatrix} L_1 \\ L_2 \end{pmatrix}. \end{aligned} \tag{9}$$

Equation (9) in its simpler form is written as

$$\dot{x_1}(t) = L_1[(y(t) - x_1(t)] + x_2 + b_0u(t) \tag{10}$$

$$\dot{x_2}(t) = L_2[(y(t) - x_1(t)]. \tag{11}$$

Figure 3a shows the developed ESO for the present HES by using Equations (10) and (11).

For the present HES, the plant to be controlled is the three-area and the estimation parameter is the area-control-error (ACE_i) in both areas which is fed as error input to the controller. Once the design of ESO for the controller is done, the implementation of the proposed 1D-ADRC is performed and is shown in Figure 3b. The proposed 1D-ADRC is based on the following control law:

$$u(t) = \frac{u_0(t) - f(t)}{b_0}$$

with

$$u_0(t) = K_p(Ref - ACE(t)). \tag{12}$$

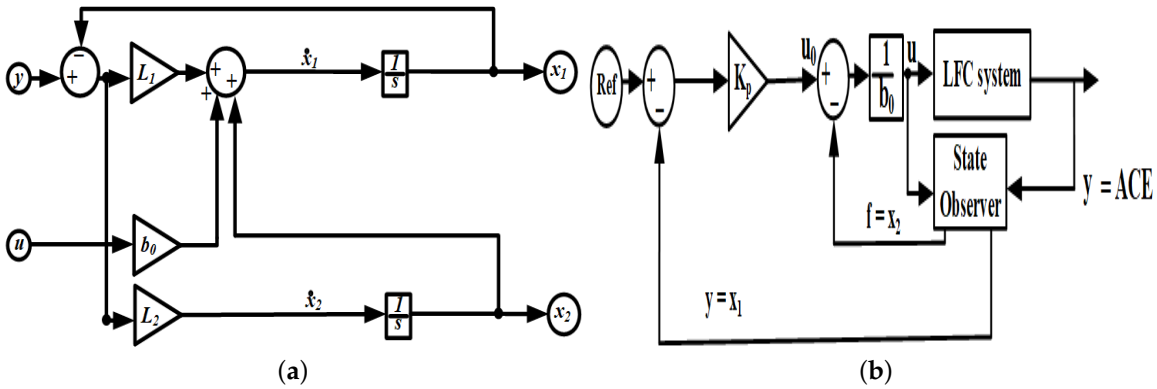


Figure 3. Proposed 1D-ADRC with ESO for the present HES. (**a**) ESO block diagram. (**b**) 1D-ADRC with ESO) model.

2.3. *Arithmetic Optimization Algorithm (AOA)*

Arithmetic is a basic constituent of a number system, and a major vital part of present mathematical analysis. The classic calculation measures used to examine numbers are arithmetic operators (multiplication, division, addition, and subtraction). We employ these basic operators as a mathematical optimization to identify the best element from a pool of potential alternatives based on particular criteria. The usage of arithmetic operators in solving arithmetic issues is the major source of inspiration for the AOA. This algorithm is a population-based meta-heuristic that solves optimization problems without the need to calculate their derivatives. The steps involved in AOA algorithms are mentioned below.

First, the AOA optimization approach starts with a randomization of set of candidate solutions (X) as presented in Matrix (13). For each iteration, the best candidate solution is deemed to be the effectively achieved solution or approximately the optimal until now. The AOA should choose the searching stage before beginning its job (i.e., exploration or exploitation). Therefore, the math-optimizer-accelerated (MOA) function is utilized in search phase, as presented in (14):

$$X = \begin{bmatrix} x_{1,1} & . & . & x_{1,j} & x_{1,n-1} & x_{1,n} \\ x_{2,1} & . & . & x_{2,j} & . & x_{2,1} \\ . & . & . & . & . & . \\ . & . & . & . & . & . \\ x_{N-1,1} & . & . & x_{N-1,j} & . & x_{N-1,n} \\ x_{N,1} & . & . & x_{N,j} & x_{N,n-1} & x_{N,n} \end{bmatrix} \tag{13}$$

$$MOA(C_Iter) = Min + C_Iter\frac{Max_Min}{M_Iter}, \tag{14}$$

where, $MOA(C_Iter)$ represents the value of the function at the ith iteration, C_Iter represents the present iteration, M_Iter represents the highest quantity of iterations. Min and Max represent the largest and smallest values of the accelerated function.

Secondly, AOA's exploration operators randomly seek different regions in order to discover a better solution by using two basic search methods, D and M, which are demonstrated in Equation (15). The MOA function is utilized for searching phase by implementing D or M for the case of $r1 > MO$, where r1 is a random number. In this stage, the operator D is constrained by $r2 < 0.5$ and the M operator is omitted unless the D operator completes its present task. To construct additional diversification courses and

investigate other sections of the search space, a probabilistic ramping coefficient is explored for the element

$$x_{i,j}(C_Iter+1) = \begin{matrix} best(x_j) \div (MOP+\epsilon) \times ((UB_j - LB_j) \times \mu + LB_j), & r2 < 0.5 \\ = best(x_j) \times MOP \times ((UB_j - LB_j) \times \mu + LB_j), & otherwise \end{matrix}, \quad (15)$$

where $x_i(C_Iter+1)$ represents the ith solution in the coming iteration, $x_{i,j}(C_Iter)$ represents the jth location of the ith solution for the present iteration and best (x_j) represents the jth location in the better-achieved solution until now, and UB_j and LB_j represent the constraints of the jth location. The μ parameter is utilized in the search operation. The math optimizer probability (MOP) is estimated by utilizing Equation (16),

$$MOP(C_Iter) = 1 - \frac{C_Iter^{1/\alpha}}{M_Iter^{1/\alpha}}, \quad (16)$$

where α is a crucial factor that determines the precision of exploitation across iterations.

Thirdly, the exploitation stage of AOA done by the MOA function for the scenario $r1$ is no larger than the present $MOA(C_Iter)$. The exploitation operators (Subtraction (S) and Addition (A)) delve deeper into the search region across numerous dense locations in order to discover a better solution by using two major search methodologies, presented in (17),

$$x_j(C_Iter+1) = \begin{matrix} best(x_j) - MOP \times ((UB_j - LB_j) \times \mu + LB_j), & r3 < 0.5 \\ = best(x_j) + MOP \times ((UB_j - LB_j) \times \mu + LB_j), & otherwise \end{matrix}. \quad (17)$$

Exploitation search operators usually try to stay out of the local search area as much as possible. This approach aids exploration search strategies in locating the best solution while maintaining the variety of candidate solutions. The flowchart for AOA working is presented in Figure 4.

The objective function is considered as the integral squared error (ISE) and given by Equation (18):

$$ISE = \int_0^T (\Delta f_i^2 + \Delta P_{tie-ij}^2).dt, i = 1,2,3. \quad (18)$$

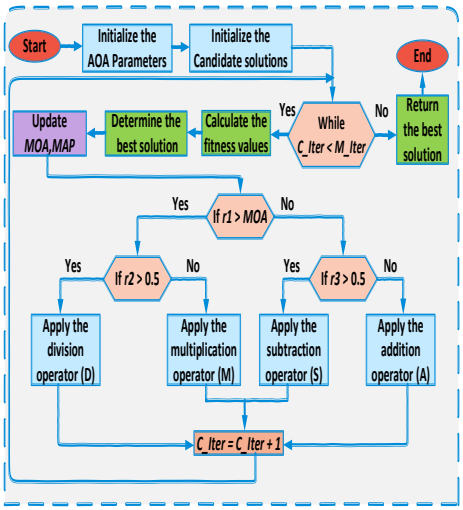


Figure 4. Flowchart for arithmetic optimization algorithm.

2.4. Modelling Tools Used

The modelling of power system is done in MATLAB 2018a platform. The optimization technique used is developed in MATLAB coding software. The parameters used for optimization algorithm are listed in Table 1.

Table 1. Optimization parameters used.

Parameter	Value
Population size	100
No. of iterations	50
Parameter lower limit	0
Parameter upper limit	100
Dimension size	6
Alpha	5
Mu	0.499
MOP_{Max}	1
MOP_{Min}	0.2

3. Result and Discussion

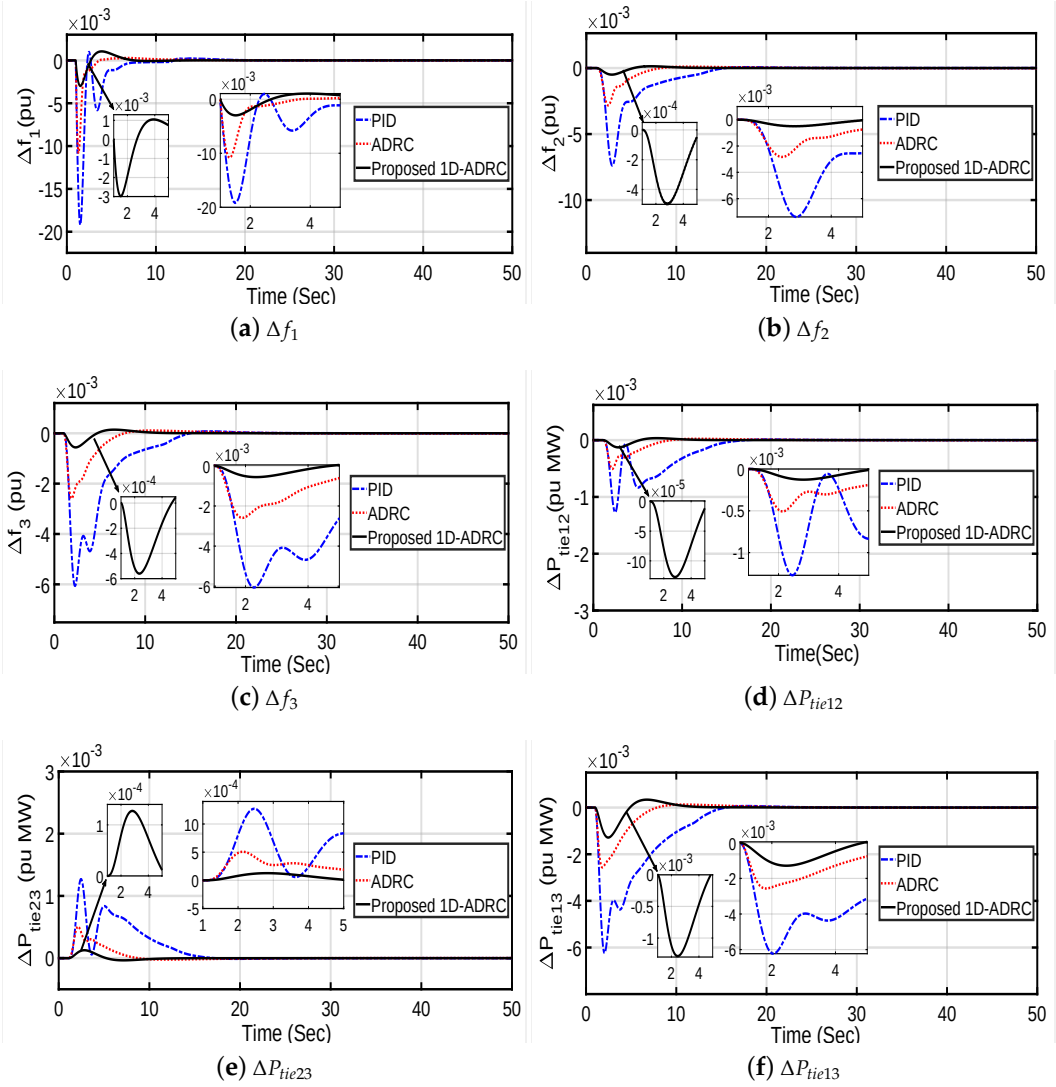
The MATLAB Simulink tool is utilized to perform the analysis on the developed power system. The step load disturbance (SLP) of 1 percent is supplied in Area 1 for nominal case studies.

3.1. Secondary Controller Selection

This section deals with the optimal secondary controller selection among different secondary considered controllers. Different controllers, such as PID [11], conventional-ADRC [30], and the proposed 1D-ADRC controllers, are assessed separately in frequency stabilization of HES. AOA is applied in adjustment of the abovementioned controller gains in line with the lesser ISE value, which is an objective function for the present study. The developed HES is simulated for each of the abovementioned controllers. The system responses (frequency and tie-line power) are attained, and displayed in Figure 5. The observation of response comparison in Figure 5 exposes the optimal performance of HES in the existence of the proposed 1D-ADRC controller.

The proposed 1D-ADRC suppresses the system deviations within the short range of overshoots and undershoots with respect to PID and conventional-ADRC. The system deviations are forced to zero steady-state values effectively. The responses are damped faster by using the proposed 1D-ADRC scheme with respect to PID and conventional ADRC.

As seen from Figure 5, the magnitude of the maximum deviation in frequency is 0.0039 p.u. with a time of settling of 7.05 s by using the proposed LFC scheme. The corresponding values for PID scheme are 0.0201 p.u with time of settling 19.41 s for frequency variation. For a conventional ADRC scheme, the frequency attributes are 0.0001 p.u with time of settling 14.3. Figure 5 shows that with the proposed ADRC scheme, the frequency deviation is limited within the $\pm 3\%$ band. The values of magnitudes of maximum overshoots, maximum undershoots, and time of settling for all the controllers are reported in Table 2. These results show that the proposed LFC-AVR scheme significantly improves the performance of the one-area hybrid power system. Furthermore, the ISE values attained for each controller, reported in Table 3, convey the least ISE value for the 1D-ADRC controller, which is a desirable condition for any power system. It is worth noting that the smaller the ISE value, the better is the overall performance of the system, and vice versa. The system deviations are minimum for 1D-ADRC controller, which is why the proposed controller has the least ISE value. Furthermore, the values noted for highest overshoot (HV), lowest undershoot (LU), and response settling (RT) in Table 2 ascertain the dominance of the 1D-ADRC controller over other considered secondary controllers.



(**a**) Δf_1 (**b**) Δf_2

(**c**) Δf_3 (**d**) ΔP_{tie12}

(**e**) ΔP_{tie23} (**f**) ΔP_{tie13}

Figure 5. Response comparison of PID, conventional-ADRC, 1D-ADRC controllers.

Table 2. Observations of Figure 5.

Parameter	Controller	LU	HV	RT
Δf_1	PID	-0.0192	0.0009	19.41
	ADRC	-0.0108	0.0003	14.3
	1D-ADRC	-0.0029	0.001	7.05
Δf_2	PID	-0.0074	6.5×10^{-5}	21.2
	ADRC	-0.0029	0.0001	18.61
	1D-ADRC	-0.0004	0.0001	8.6
Δf_3	PID	-0.0061	7.4×10^{-5}	23.02
	ADRC	-0.0026	0.0001	20.12
	1D-ADRC	-0.0005	0.0001	9.94
ΔP_{tie12}	PID	-0.0013	1.1×10^{-5}	23.05
	ADRC	-0.0005	2.3×10^{-5}	18.19
	1D-ADRC	-0.0001	3.5×10^{-5}	8.56
ΔP_{tie23}	PID	-1.1×10^{-5}	0.0013	23.20
	ADRC	-2.3×10^{-5}	0.0005	20.12
	1D-ADRC	-3.5×10^{-5}	0.0001	9.68

Table 2. *Cont.*

Parameter	Controller	LU	HV	RT
ΔP_{tie13}	PID	−0.0062	6.4×10^{-5}	23.54
	ADRC	−0.0025	0.0001	20.78
	1D-ADRC	−0.001	0.0003	10.91

Table 3. ISE value for different controllers.

Controller	ISE Value (Objective Function)
PID	0.00034
conventional-ADRC	0.00019
1D-ADRC	0.00014

3.2. Controller Robustness against Random Load Disturbances

The load demand is usually uncertain in a realistic power system. In order to reflect such practicality into the developed HES, Area 1 and Area 3 are supplied with the random load perturbation (RLP). The RLP provided with these two areas is displayed in Figure 6a. As in the above case, the secondary controllers, viz. PID, conventional ADRC, and 1D-ADRC are assessed separately for these random disturbances. The AOA approach is applied in adjusting the controller gains. The RLP-provided HES is simulated for each controller mentioned above. The system responses are achieved and are accessible in Figure 6b–d. The assessment of the responses in Figure 6b–d reflects that the random disturbances are more effectively handled by the proposed 1D-ADRC controller.

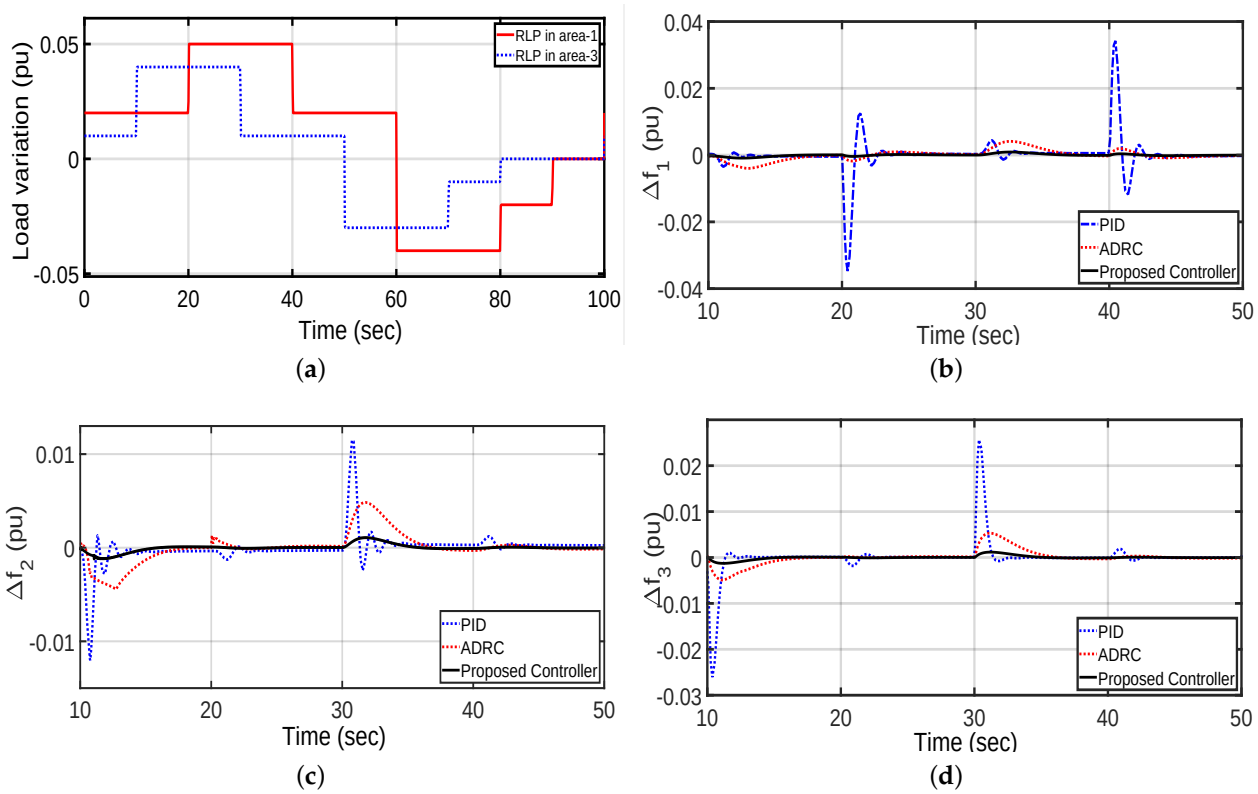


Figure 6. Response comparison of PID, conventional ADRC, and 1D-ADRC against random disturbances. (**a**) RLP Pattern; (**b**) Δf_1; (**c**) Δf_2; (**d**) Δf_3.

4. Effect of EVs on the HES

In this section, the nominal test system discussed in Section 2.1 is integrated with modern day EVs in different buses of each area. Alternate plugging of EVs is performed in each area, and the performance of the HES is evaluated after the interconnection of EVs. The responses obtained in this case are compared with the nominal case (Figure 5). The system parameters are optimized by using AOA in this case as well. Based on the response comparison and ISE values obtained in each case, the optimal location of EVs for each area of the HES is determined.

4.1. Modelling of EV

The collaborative simulation model for EV utilised in the current analysis is portrayed in Figure 7. The battery charger is accountable for ensuring that power is exchanged between the grid and battery. The use of batteries for frequency mitigation is one of the main advantages of using EVs for grid integration. Bi-directional power electronic converters (BPEC) are employed to integrate EVs to the grid. A scenario can play out in which EVs can be unexpectedly disengaged from the grid, leading to an undesired frequency outcome, which is not recommended for power systems. As a result, frequency is capped to a range of ±10 mHz. The capability and supervision of an EV are correlated to its charging/discharging conduct, which has a significant effect on the amount of regulatory duty allocated to the EV [26]. The regulatory control is governed by the capacity and power-load discrepancy. EVs that assist in regulatory activities usually require sufficient time to charge the batteries to the desirable level. Any power disparity will be broken into two portions because all generating units, including EVs, are accountable for regulation. A portion of the job will be done by all of the generating units in a given region, and the remainder will be addressed by BCM.The value of droop co-efficient is R_{EV} is 2.4 Hz/MW. The incremental power deviation in EVs is stated by ΔP_{EV}. The maximum and minimum power output of EVs are denoted by P_{AG}^{max} and P_{AG}^{min}, given in (19) and (20):

$$P_{AG}^{max} = +(\frac{1}{N_{EV}})(\Delta P_{EVi}) \tag{19}$$

$$P_{AG}^{min} = -(\frac{1}{N_{EV}})(\Delta P_{EVi}). \tag{20}$$

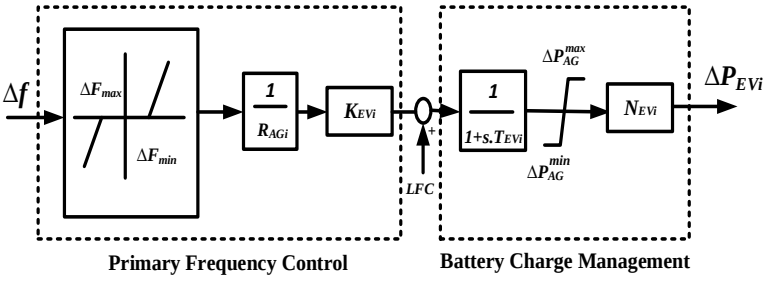


Figure 7. Simulation model of EV.

4.2. Evaluation of Optimal Location of EVs

The authors of [45] have demonstrated the optimal placement of distributed photo-voltaic systems and EV charging stations. For evaluating the optimal location of EVs in the HES, a considerable number of EVs are initially connected in each area of the HES separately. The responses in each case are obtained. The responses obtained in this case are compared with that of the responses obtained in the nominal case (Figure 5).The study is divided in the following steps.

4.2.1. EVs Connected in Area 1 Only

Here, 1000 EVs are connected to the nominal system in Area 1 only, and the system is simulated for proposed 1D-ADRC optimized with AOA technique. The responses for frequency deviations in all three areas are obtained, and the values of ISE as well. Figure 8 shows the comparison of frequency deviations obtained when N_{EV} = 1000 are connected in Area 1 and the the nominal system frequency deviations (Figure 5).

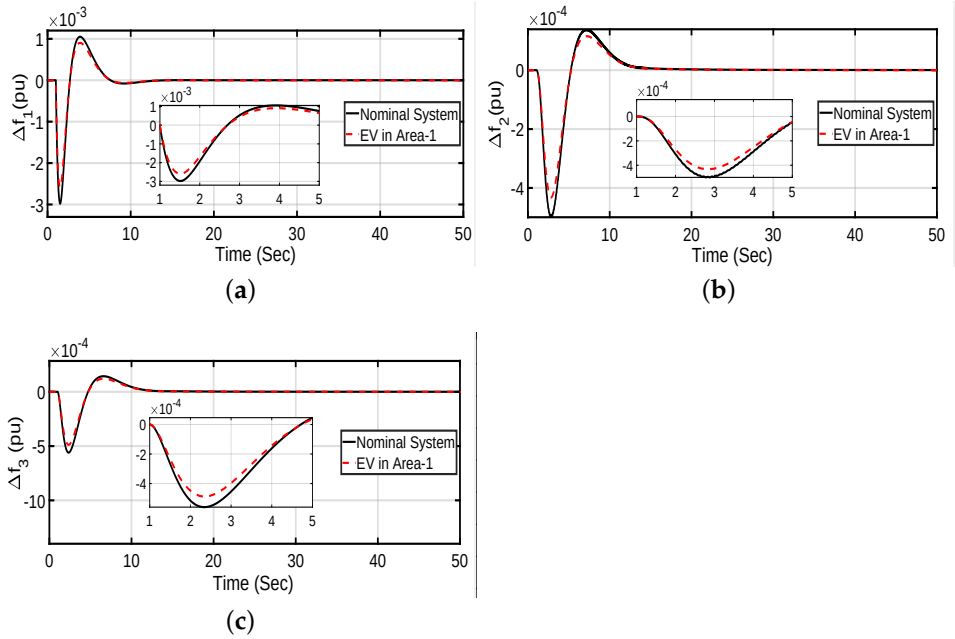


Figure 8. Response comparison when EVs are connected in Area 1 only. (**a**) Δf_1; (**b**) Δf_2; (**c**) Δf_3.

4.2.2. EVs Connected in Area 2 Only

Here, 1000 EVs are connected to the nominal system in Area 2 only and the system is simulated for a proposed 1D-ADRC optimized with the AOA technique. The responses for frequency deviations in all three areas are obtained and the values of ISE are obtained as well. Figure 9 shows the comparison of frequency deviations obtained when N_{EV} = 1000 are connected in Area 2 and the the nominal system frequency deviations (Figure 5).

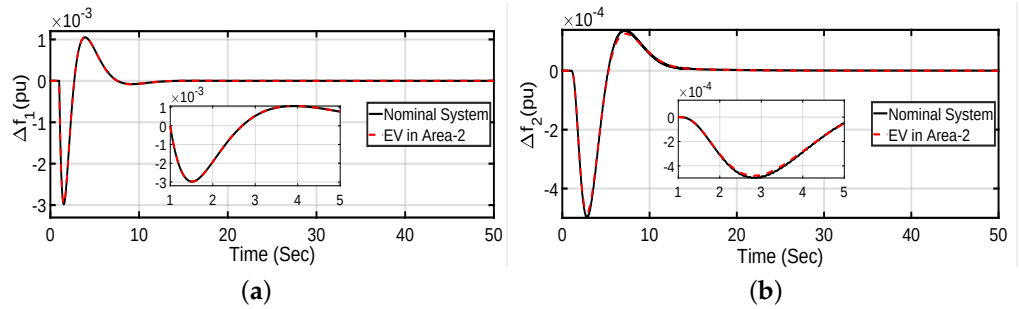
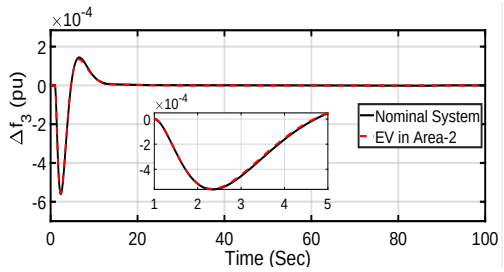


Figure 9. *Cont.*

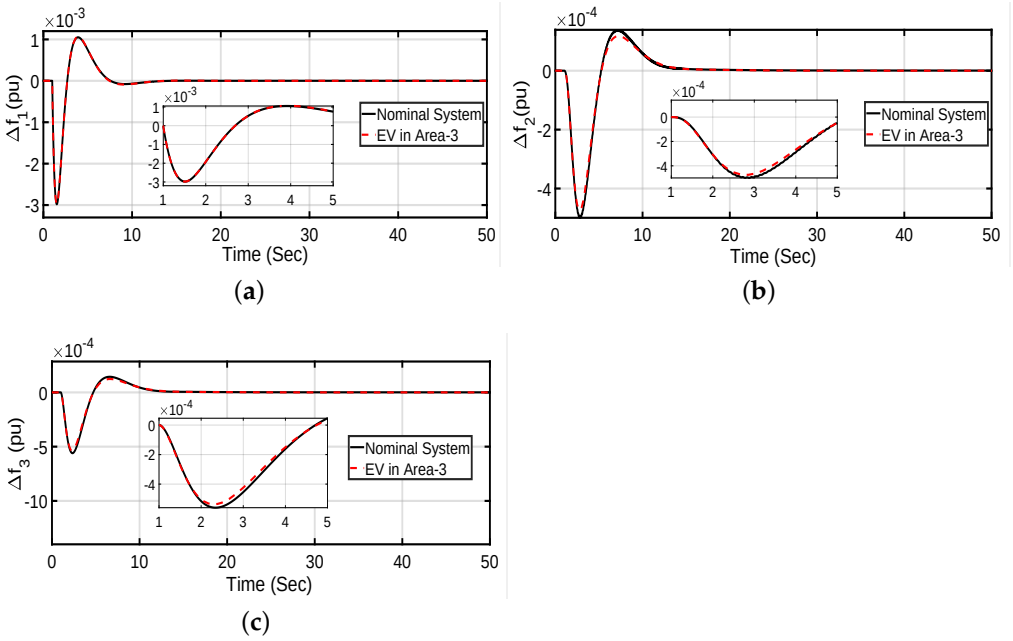


(**c**)

Figure 9. Response comparison when EVs are connected in Area 2 only. (**a**) Δf_1; (**b**) Δf_2; (**c**) Δf_3.

4.2.3. EVs Connected in Area 3 Only

Here, 1000 EVs are connected to the nominal system in Area 3 only, and the system is simulated for a proposed 1D-ADRC optimized with AOA technique. The responses for frequency deviations in all the three areas are obtained and the values of ISE as well. Figure 10 shows the comparison of frequency deviations obtained when N_{EV} = 1000 are connected in Area 3, and the the nominal system frequency deviations (Figure 5).



(**a**) (**b**)

(**c**)

Figure 10. Response comparison when EVs are connected in Area 3 only. (**a**) Δf_1; (**b**) Δf_2; (**c**) Δf_3.

4.2.4. EVs Connected in Area 1 and Area 2 Only

Here, 1000 EVs are connected to the nominal system in Area 1 and Area 2, and the system is simulated for a proposed 1D-ADRC optimized with the AOA technique. The responses for frequency deviations in all three areas are obtained, and the values of ISE are obtained as well. Figure 11 shows the comparison of frequency deviations obtained when N_{EV} = 1000 are connected in Area 1 and Area 2, and the the nominal system frequency deviations (Figure 5).

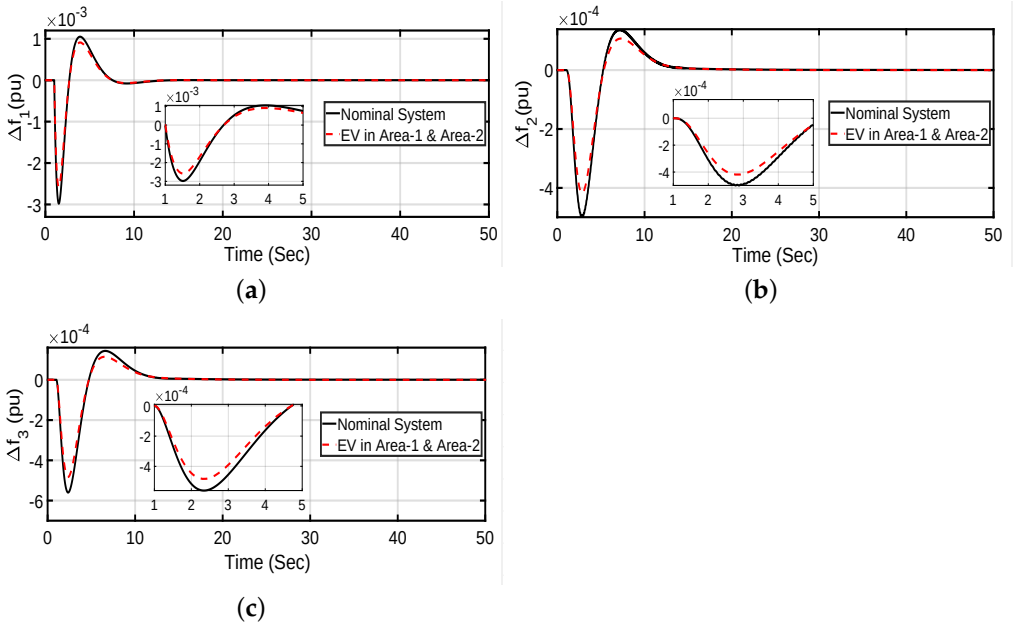


Figure 11. Response comparison when EVs are connected in Area 1 and Area 2 only. (**a**) Δf_1; (**b**) Δf_2; (**c**) Δf_3.

4.2.5. EVs Connected in Area 2 and Area 3 Only

In this study, the EVs are connected in Area 2 and Area 3 of nominal system. The 1000 EVs are taken in both areas. The EV-connected HES is simulated in the presence of the 1D-ADRC controller. The system responses are attained, and are accessible in Figure 12. The corresponding ISE values are also achieved. Figure 12 shows the comparison of frequency deviations obtained when EVs are connected in Area 2 and Area 3 with the nominal system frequency deviations (without EVs (Figure 5).

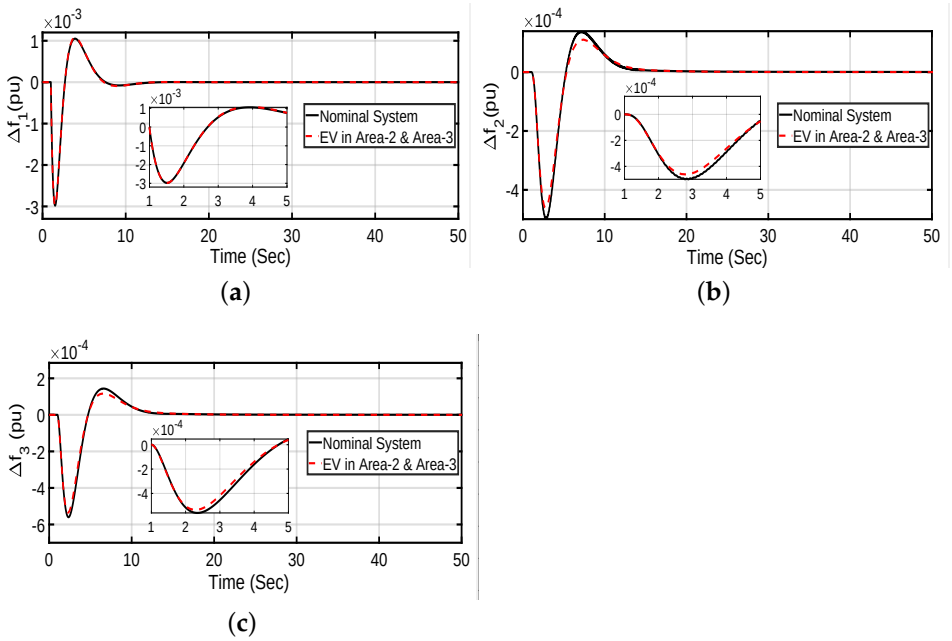


Figure 12. Response comparison when EVs are connected in Area 2 and Area 3 only. (**a**) Δf_1; (**b**) Δf_2; (**c**) Δf_3.

4.2.6. EVs Connected in Area 1 and Area 3 Only

In this study, the EVs are connected in Area 1 and Area 3 of nominal system. The 1000 EVs are taken in both areas. The EV-connected HES is simulated in the presence of the 1D-ADRC controller. The system responses are attained, and are accessible in Figure 13. The corresponding ISE values are also achieved. Figure 13 shows the comparison of frequency deviations obtained when the EVs are connected in Area 2 and Area 3 with the nominal system frequency deviations (without EVs (Figure 5).

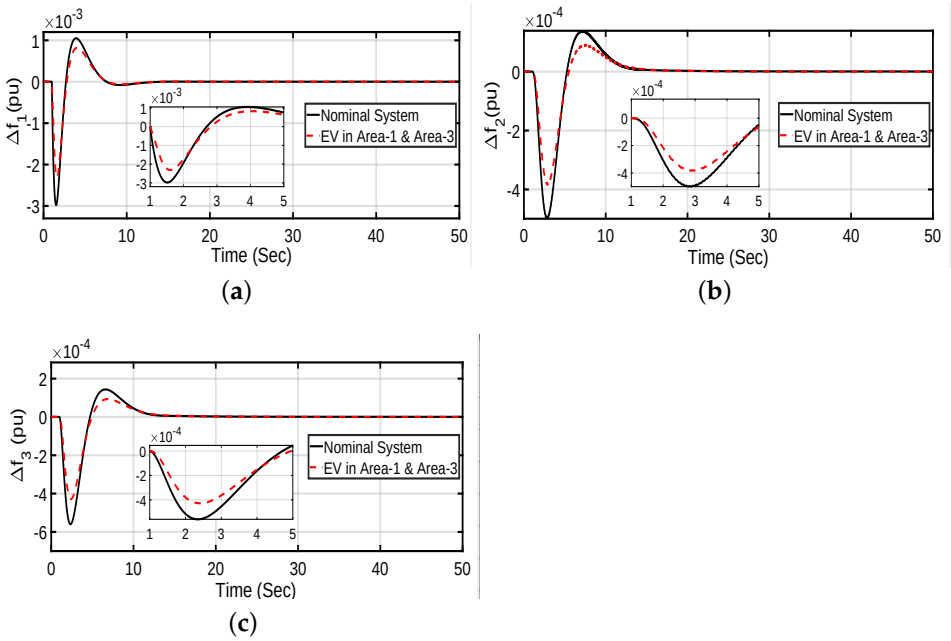


Figure 13. Response comparison when EVs are connected in Area 1 and Area 3 only. (**a**) Δf_1; (**b**) Δf_2; (**c**) Δf_3.

4.2.7. EVs Connected in All Three Areas

This study is performed by connecting EVs in all three areas. The 1000 EVs are taken into consideration, the same as in the above discussed cases. The system is simulated for proposed 1D-ADRC controller optimized with the AOA technique. The responses for frequency deviations in all three areas are obtained and the values of ISE as well. The responses attained for EV-connected HES are accessible in Figure 14. Figure 14 shows the comparison of frequency deviations obtained when EVs are connected in all three areas with the nominal system frequency deviations (without EVs) (Figure 5).

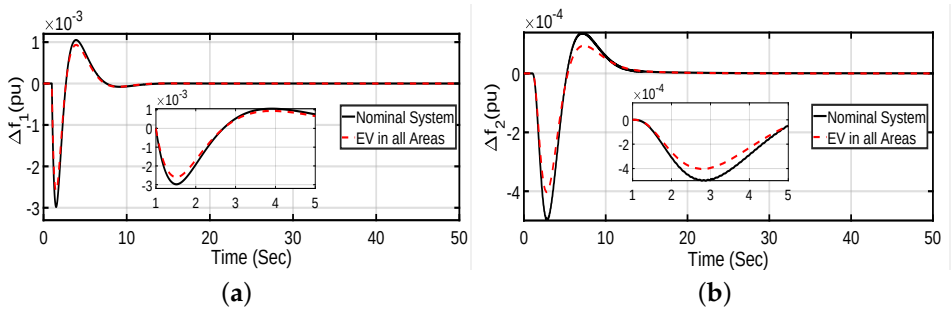
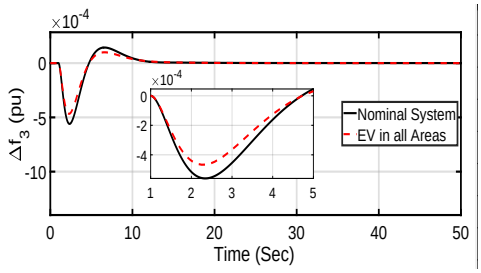


Figure 14. *Cont.*



(**c**)

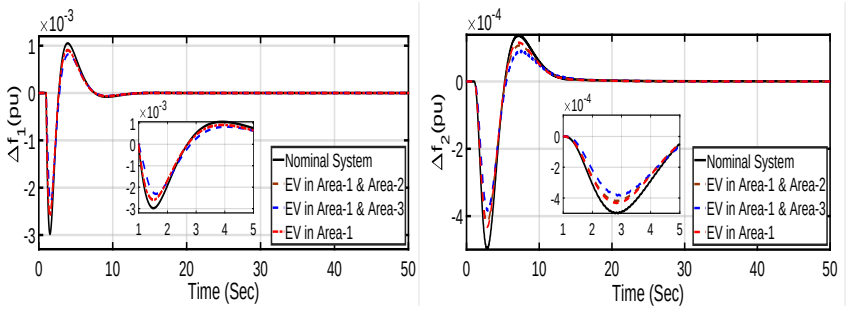
Figure 14. Response comparison when EVs are connected in all the three areas. (**a**) Δf_1; (**b**) Δf_2; (**c**) Δf_3.

4.3. Inference from Section 4.2

Comparative analysis of the different cases studied in Section 4.2 shows a critical scenario when certain EVs are connected with the power system in different areas. As can be seen from the comparison of all the cases, the system deviations are well suppressed when EVs are connected in Area 1 and Area 3. The same is validated by the ISE values obtained in Table 4 when EVs are connected in Area 1 and Area 3. However, the other two cases when EVs are connected in Area 1 only and Area 1 and Area 2 also show a prominent improvement in system performance. Thus, for a more profound analysis, the three cases when EVs are connected in Area 1 only, Area 1 and Area 2, Area 1 and Area 3 are compared separately. Figure 15 show the comparison in these cases. The comparative analysis in these cases concludes that the improvement of the system performance is attained when EVs are connected in Area 1 and Area 3 of the HES (represented by blue dotted lines in Figure 15) with ISE value of 0.00012673. Thus, upon thorough investigation of system deviation comparison and ISE values, it is concluded that when EVs are connected in Area 1 and Area 3 of the power system, the performance of the power system is improved with respect to other cases discussed in Section 4.2. Hence, the optimal location of EVs for the HES obtained is when EVs are connected in Area 1 and Area 3.

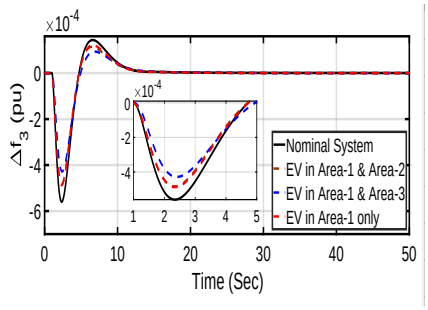
Table 4. ISE value for AOA optimized 1D-ADRC controlled HES for different combination of EVs.

Combination	ISE Value (Objective Function)
EVs in Area 1 only	0.00012760
EVs in Area 2 only	0.00014579
EVs in Area 3 only	0.00014604
EVs in Area 1 and Area 2	0.00012774
EVs in Area 2 and Area 3	0.00014588
EVs in Area 1 and Area 3	0.00012673
EVs in all three areas	0.00012804



(**a**) (**b**)

Figure 15. *Cont.*



(**c**)

Figure 15. Response comparison when EVs are connected Area 1 only, Area 1 and Area 2, Area 1 and Area 3 of the HES. (**a**) Δf_1; (**b**) Δf_2; (**c**) Δf_3.

4.4. Role of EVs in Multi-Energy System

In this analysis, 1000 EVs [46] are connected to Area 1 in addition to conventional thermal (CT) and solar thermal (ST) systems. The developed multi-energy system is provided with optimal 1D-ADRC as the secondary controller. The proposed controller capably handles the load disturbance within the stability regions. The uneven load disturbance is given to Area 1, shown in Figure 16i. The load disturbance is given considering the practical scenario.

The system deviation in terms of frequency against the random load is presented in Figure 16ii. The inference from Figure 16ii illustrates that with the increase or decrease in load, the frequency decreases with increase in load demand and vice versa. With this, the generation sources are forced to increase or decrease the power as per load demand, which in turn maintains the frequency constant at nominal value.

The generation responses for different energy sources in Area 1 are presented in Figure 16iii–v. To maintain the frequency constant against load change, the EVs rapidly raise their delivering or discharging power, which is clearly visible in Figure 16iii. EVs act as a generation source for the negative cycle of frequency deviation and load for positive cycle. The charging and discharging of the energy continues until the frequency attains a nominal value, thereby also reducing the burden on other energy sources. The generation response of ST is shown in Figure 16iv, whereas Figure 16v showcases the generation response of conventional thermal system in response to the continuous load change. The EV response is considerably more rapid than other energy sources.

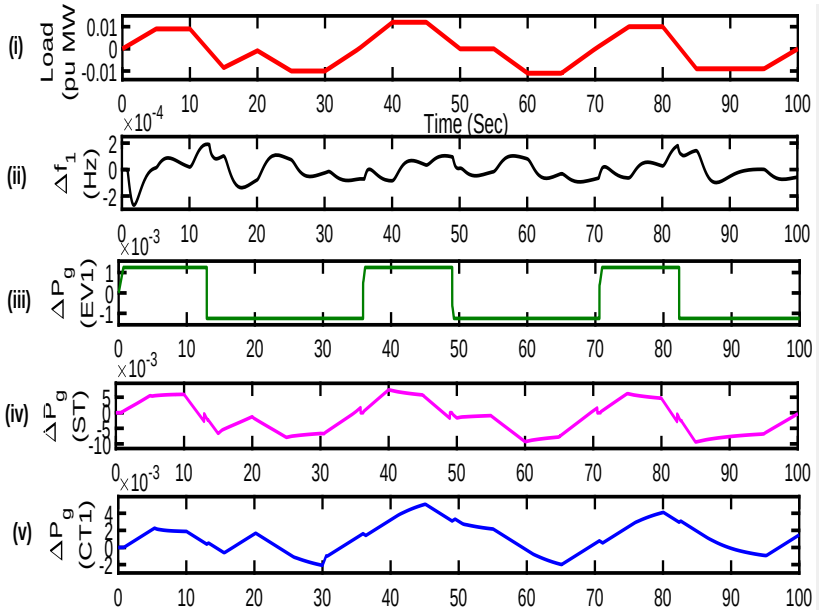


Figure 16. Generation power of multi-energy sources in Area 1.

5. Conclusions

A modified disturbance rejection-based controller is applied for a power system which showed a considerable improvement in the system performance with respect to the already established control schemes. The proposed control scheme is tested successfully on a standard IEEE-39 bus system. The proposed controller strategy has forced the system dynamic responses to perish well within defined limits after any disturbance is applied to the system. The superiority of the proposed control scheme for mitigating the system deviations under varying load conditions is evaluated as well. The proposed controller has a much faster response and is robust enough to system uncertainties and disturbances. The present work has shown the advantages of connecting EVs in the form of V2G with the power system. It has been demonstrated that EVs aid in stabilizing the power system against disturbances by supporting the power system during load demand variations. Thus, the EVs reduce burden on power system-generating components. The present work has come up with a novel idea of allocation of EVs on the power system based on the performance improvement and reduction in steady-state errors by using EVs for the developed power system. As such, the optimal location of connecting EVs with the power system is evaluated.

6. Future Scope

A new concept of power system control strategy and its application is successfully implemented in the present work. This work pressures research engineers to move out of conventional controller schemes in such fields and begin to explore this modern digital control technology to address the shortcomings of the conventional technologies.

Author Contributions: Conceptualization, Z.F., S.S., A.R. and T.S.U.; methodology, Z.F., S.S., A.R. and S.M.S.H.; software, Z.F.; validation, Z.F., S.S., A.R. and S.M.S.H.; formal analysis, Z.F., A.R., S.M.S.H. and T.S.U.; investigation, Z.F., S.S., A.R. and T.S.U.; resources, A.R.; data curation, Z.F. and A.R.; writing—original draft preparation, Z.F.; writing—review and editing, A.R., S.M.S.H. and T.S.U.; visualization, Z.F.; supervision, A.R., S.M.S.H. and T.S.U.; funding acquisition, T.S.U. All authors have read and agreed to the published version of the manuscript.

Funding: This research received no external funding.

Institutional Review Board Statement: Not Applicable.

Informed Consent Statement: Not Applicable.

Data Availability Statement: All the data generated in present work is already available in the reported manuscript or cited accordingly.

Conflicts of Interest: The authors declare no conflict of interest.

Abbreviations

LFC	Load Frequency Control
HES	Hybrid Energy System
PID	Proportional Integral Derivative
ADRC	Active Disturbance Rejection Controller
AOA	Arithmetic Optimization22 Algorithm
EV	Electric Vehicle
V2G	Vehicle-to-Grid
ISE	Integral Squarred Error
RES	Renewable Energy Sources
RLP	Random Load Perturbation

References

1. Ustun, T.S.; Hashimoto, J.; Otani, K. Impact of Smart Inverters on Feeder Hosting Capacity of Distribution Networks. *IEEE Access* **2019**, *7*, 163526–163536. [CrossRef]
2. Shangguan, X.C.; He, Y.; Zhang, C.K.; Jiang, L.; Wu, M. Load frequency control of time-delayed power system based on event-triggered communication scheme. *Appl. Energy* **2022**, *308*, 118294. [CrossRef]
3. Latif, A.; Hussain, S.S.; Das, D.C.; Ustun, T.S. Double stage controller optimization for load frequency stabilization in hybrid wind-ocean wave energy based maritime microgrid system. *Appl. Energy* **2021**, *282*, 116171. [CrossRef]
4. Farooq, Z.; Rahman, A.; Hussain, S.M.S.; Ustun, T.S. Power Generation Control of Renewable Energy Based Hybrid Deregulated Power System. *Energies* **2022**, *15*, 517. [CrossRef]
5. Nadeem, F.; Aftab, M.A.; Hussain, S.M.S.; Ali, I.; Tiwari, P.K.; Goswami, A.K.; Ustun, T.S. Virtual Power Plant Management in Smart Grids with XMPP Based IEC 61850 Communication. *Energies* **2019**, *12*, 2398. [CrossRef]
6. Ranjan, S.; Das, D.C.; Latif, A.; Sinha, N.; Hussain, S.M.S.; Ustun, T.S. VMaiden Voltage Control Analysis of Hybrid Power System with Dynamic Voltage Restorer. *IEEE Access* **2021**, *9*, 60531–60542. [CrossRef]
7. Elgerd, O.I.; Fosha, C.E. Optimum Megawatt-Frequency Control of Multiarea Electric Energy Systems. *IEEE Trans. Power Appar. Syst.* **1970**, *PAS-89*, 556–563. [CrossRef]
8. Performance comparison of several classical controllers in AGC for multi-area interconnected thermal system. *Int. J. Electr. Power Energy Syst.* **2011**, *33*, 394–401. [CrossRef]
9. Debbarma, S.; Chandra Saikia, L.; Sinha, N. Solution to automatic generation control problem using firefly algorithm optimized I^{λ} D^{μ}) controller. *ISA Trans.* **2014**, *53*, 358–366. [CrossRef]
10. Rahman, A.; Saikia, L.C.; Sinha, N. Automatic generation control of an unequal four-area thermal system using biogeography-based optimised 3DOF-PID controller. *Gener. Transm. Distrib. IET* **2016**, *10*, 4118–4129. [CrossRef]
11. Aditya. Design of Load Frequency Controllers Using Genetic Algorithm for Two Area Interconnected Hydro Power System. *Electr. Power Components Syst.* **2003**, *31*, 81–94. [CrossRef]
12. Arya, Y.; Kumar, N. AGC of a multi-area multi-source hydrothermal power system interconnected via AC/DC parallel links under deregulated environment. *Int. J. Electr. Power Energy Syst.* **2016**, *75*, 127–138. [CrossRef]
13. Subbaramaiah, k. Improvement of dynamic performance of SSSC and TCPS based hydrothermal system under deregulated scenario employing PSO based dual mode controller. *Eur. J. Sci. Res* **2011**, *57*, 230–243.
14. Shankar, R.; Bhushan, R.; Chatterjee, K. Small-signal stability analysis for two-area interconnected power system with load frequency controller in coordination with FACTS and energy storage device. *Ain Shams Eng. J.* **2016**, *7*, 603–612. [CrossRef]
15. Pradhan, P.C.; Sahu, R.K.; Panda, S. Firefly algorithm optimized fuzzy PID controller for AGC of multi-area multi-source power systems with UPFC and SMES. *Eng. Sci. Technol. Int. J.* **2016**, *19*, 338–354. [CrossRef]
16. Lee, D.J.; Wang, L. Small-Signal Stability Analysis of an Autonomous Hybrid Renewable Energy Power Generation/Energy Storage System Part I: Time-Domain Simulations. *IEEE Trans. Energy Convers.* **2008**, *23*, 311–320. [CrossRef]
17. Dey, P.P.; Das, D.C.; Latif, A.; Hussain, S.M.S.; Ustun, T.S. Active Power Management of Virtual Power Plant under Penetration of Central Receiver Solar Thermal-Wind Using Butterfly Optimization Technique. *Sustainability* **2020**, *12*, 6979. [CrossRef]
18. Chauhan, A.; Upadhyay, S.; Khan, M.T.; Hussain, S.M.S.; Ustun, T.S. Performance Investigation of a Solar Photovoltaic/Diesel Generator Based Hybrid System with Cycle Charging Strategy Using BBO Algorithm. *Sustainability* **2021**, *13*, 8048. [CrossRef]
19. Farooq, Z.; Rahman, A.; Lone, S.A. Load frequency control of multi-source electrical power system integrated with solar-thermal and electric vehicle. *Int. Trans. Electr. Energy Syst.* **2021**, *31*, e12918. [CrossRef]
20. Rahman, A.; Saikia, L.C.; Sinha, N. Automatic generation control of an interconnected two-area hybrid thermal system considering dish-stirling solar thermal and wind turbine system. *Renew. Energy* **2017**, *105*, 41–54. [CrossRef]
21. Hemission, B. Improved Frequency Control Strategies for Geothermal Power Plants. Master's Thesis, Chalmers University of Technology, Göteborg, Sweden, 2014.
22. Tasnin, W.; Saikia, L.C. Performance comparison of several energy storage devices in deregulated AGC of a multi-area system incorporating geothermal power plant. *IET Renew. Power Gener.* **2018**, *12*, 761–772. [CrossRef]
23. Niekurzak, M.; Lewicki, W.; Drożdż, W.; Miązek, P. Measures for Assessing the Effectiveness of Investments for Electricity and Heat Generation from the Hybrid Cooperation of a Photovoltaic Installation with a Heat Pump on the Example of a Household. *Energies* **2022**, *15*, 6089. [CrossRef]
24. Lan, T.; Jermsittiparsert, K.; Alrashood, S.T.; Rezaei, M.; Al-Ghussain, L.; Mohamed, M.A. An advanced machine learning based energy management of renewable microgrids considering hybrid electric vehicles' charging demand. *Energies* **2021**, *14*, 569. [CrossRef]
25. Li, C.; Cao, Y.; Zhang, M.; Wang, J.; Liu, J.; Shi, H.; Geng, Y. Hidden Benefits of Electric Vehicles for Addressing Climate Change. *Sci. Rep.* **2015**, *5*, 9213. [CrossRef]
26. Liu, H.; Huang, K.; Yang, Y.; Wei, H.; Ma, S. Real-time vehicle-to-grid control for frequency regulation with high frequency regulating signal. *Prot. Control Mod. Power Syst.* **2018**, *13*, 1–8. [CrossRef]
27. Farooq, Z.; Rahman, A.; Lone, S.A. System dynamics and control of EV incorporated deregulated power system using MBO-optimized cascaded ID-PD controller. *Int. Trans. Electr. Energy Syst.* **2021**, *31*, e13100. [CrossRef]

28. Hussain, I.; Das, D.C.; Sinha, N.; Latif, A.; Hussain, S.M.S.; Ustun, T.S. Performance Assessment of an Islanded Hybrid Power System with Different Storage Combinations Using an FPA-Tuned Two-Degree-of-Freedom (2DOF) Controller. *Energies* **2020**, *13*, 5610. [CrossRef]
29. Latif, A.; Hussain, S.M.S.; Das, D.C.; Ustun, T.S. Design and Implementation of Maiden Dual-Level Controller for Ameliorating Frequency Control in a Hybrid Microgrid. *Energies* **2021**, *14*, 2418. [CrossRef]
30. Rahman, M.M.; Chowdhury, A.H. Comparative study of ADRC and PID based Load Frequency Control. In Proceedings of the 2015 International Conference on Electrical Engineering and Information Communication Technology (ICEEICT), Savar, Dhaka, 21–23 May 2015; pp. 1–5.
31. Ranjan, S.; Das, D.C.; Sinha, N.; Latif, A.; Hussain, S.M.S.; Ustun, T.S. Voltage stability assessment of isolated hybrid dish-stirling solar-thermal-diesel microgrid with STATCOM using mine blast algorithm. *Electr. Power Syst. Res.* **2021**, *196*, 107239. [CrossRef]
32. Tang, Y.; Bai, Y.; Huang, C.; Du, B. Linear active disturbance rejection-based load frequency control concerning high penetration of wind energy. *Energy Convers. Manag.* **2015**, *95*, 259–271. [CrossRef]
33. Safiullah, S.; Rahman, A.; Ahmad Lone, S. Optimal control of electrical vehicle incorporated hybrid power system with second order fractional-active disturbance rejection controller. *Optim. Control. Appl. Methods* **2021**. [CrossRef]
34. Latif, A.; Hussain, S.M.S.; Das, D.C.; Ustun, T.S. Optimum Synthesis of a BOA Optimized Novel Dual-Stage PI − (1 + ID) Controller for Frequency Response of a Microgrid. *Energies* **2020**, *13*, 3446. [CrossRef]
35. Singh, S.; Chauhan, P.; Aftab, M.A.; Ali, I.; Hussain, S.M.S.; Ustun, T.S. Optimal Voltage–Frequency Regulation in Distributed Sustainable Energy-Based Hybrid Microgrids with Integrated Resource Planning. *Energies* **2020**, *13*, 1295. [CrossRef]
36. Barik, A.K.; Das, D.C.; Latif, A.; Hussain, S.M.S.; Ustun, T.S. Cost Optimization of a Stand-Alone Hybrid Energy System with Fuel Cell and PV. *Energies* **2021**, *14*, 2735. [CrossRef]
37. Ulutas, A.; Altas, I.H.; Onen, A.; Ustun, T.S. Neuro-Fuzzy-Based Model Predictive Energy Management for Grid Connected Microgrids. *Electronics* **2020**, *9*, 900. [CrossRef]
38. Safiullah, S.; Rahman, A.; Lone, S.A. A second-order ADRC for Synchronized Frequency-Voltage Mitigation of EV Integrated Power System. *IETE J. Res.* **2022**, 1–16. [CrossRef]
39. Safiullah, S.; Rahman, A.; Lone, S.A.; Hussain, S.S.; Ustun, T.S. Robust frequency–voltage stabilization scheme for multi-area power systems incorporated with EVs and renewable generations using AI based modified disturbance rejection controller. *Energy Rep.* **2022**, *8*, 12186–12202. [CrossRef]
40. Safiullah, S.; Rahman, A.; Lone, S.A. A 2nd order Active Disturbance Rejection Controller for coordinated frequency-voltage control of deregulated hybrid power system with optimal electric-vehicle integration. *Electr. Power Syst. Res.* **2022**, *210*, 108129. [CrossRef]
41. Safiullah, S.; Rahman, A.; Lone, S.A. State-observer based IDD controller for concurrent frequency-voltage control of a hybrid power system with electric vehicle uncertainties. *Int. Trans. Electr. Energy Syst.* **2021**, *31*, e13083. [CrossRef]
42. Safiullah, S.; Rahman, A. Performance Evaluation of Hybrid Power System Incorporating Electric-Vehicles. *Distrib. Gener. Altern. Energy J.* **2022**, *37*, 1055–1082. [CrossRef]
43. Laith, A.; Diabat, A.; Mirjalali, S.; Elaziz, M.; Gandomi, A. The Arithmetic Optimization Algorithm. *Comput. Methods Appl. Mech. Engine* **2021**, *376*, 113609.
44. Liao, K.; Xu, Y. A robust load frequency control scheme for power systems based on second-order sliding mode and extended disturbance observer. *IEEE Trans. Ind. Inform.* **2017**, *14*, 3076–3086. [CrossRef]
45. Yenchamchalit, K.; Kongjeen, Y.; Prabpal, P.; Bhumkittipich, K. Optimal Placement of Distributed Photovoltaic Systems and Electric Vehicle Charging Stations Using Metaheuristic Optimization Techniques. *Symmetry* **2021**, *13*, 2378. [CrossRef]
46. Farooq, Z.; Rahman, A.; Lone, S.A. Power generation control of restructured hybrid power system with FACTS and energy storage devices using optimal cascaded fractional-order controller. *Optim. Control. Appl. Methods* **2022**, *43*, 757–786. [CrossRef]